Original Research

C.A. Garcia*
B.J. Andraski
D.A. Stonestrom
C.A. Cooper
J. Šimůnek
S.W. Wheatcraft

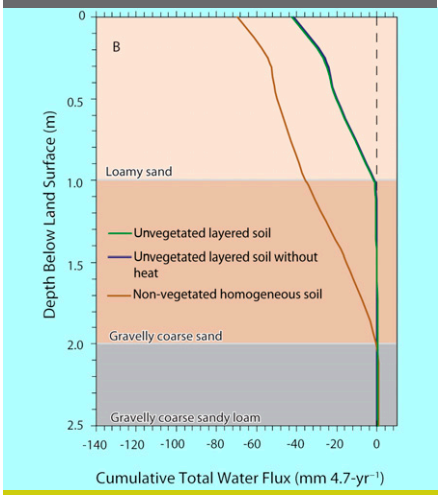

Coupled and separate effects of vegetative and thermal-gradient contributions to arid soil-water movement are evaluated using simulations with and without vegetation and thermal forcing. Thermal gradients interact with root uptake to limit sub-root-zone percolation and provide supplemental moisture to plants in late summer.

C.A. Garcia, B.J. Andraski, U.S. Geological Survey, 2730 N. Deer Run Road, Carson City, NV 89701; D.A. Stonestrom, U.S. Geological Survey, 345 Middlefield Road, Menlo Park, CA 94025; C.A. Cooper, Desert Research Institute, 2215 Raggio Parkway, Reno, NV 89512; J. Šimůnek, Dep. of Environmental Sciences, Univ. of California Riverside, Riverside, CA, 92521; S.W. Wheatcraft, Wheatcraft & Associates LLC, 3155 Heatheridge Lane, Reno, NV 89509. *Corresponding author (cgarcia@usgs.gov).

Vadose Zone J. 10:552–564
doi:10.2136/vzj2010.0023
Received 12 Feb. 2010.
Posted online 30 Mar. 2011.

Interacting Vegetative and Thermal Contributions to Water Movement in Desert Soil

Thermally driven water-vapor flow can be an important component of total water movement in bare soil and in deep unsaturated zones, but this process is often neglected when considering the effects of soil–plant–atmosphere interactions on shallow water movement. The objectives of this study were to evaluate the coupled and separate effects of vegetative and thermal-gradient contributions to soil water movement in desert environments. The evaluation was done by comparing a series of simulations with and without vegetation and thermal forcing during a 4.7-yr period (May 2001–December 2005). For vegetated soil, evapotranspiration alone reduced root-zone (upper 1 m) moisture to a minimum value (25 mm) each year under both isothermal and nonisothermal conditions. Variations in the leaf area index altered the minimum storage values by up to 10 mm. For unvegetated isothermal and nonisothermal simulations, root-zone water storage nearly doubled during the simulation period and created a persistent driving force for downward liquid fluxes below the root zone (total net flux ~1 mm). Total soil water movement during the study period was dominated by thermally driven vapor fluxes. Thermally driven vapor flow and condensation supplemented moisture supplies to plant roots during the driest times of each year. The results show how nonisothermal flow is coupled with plant water uptake, potentially influencing ecohydrologic relations in desert environments.

Abbreviations: ET, evapotranspiration; LAI, leaf area index; PET, potential evapotranspiration.

Vegetation provides important controls on hydrologic fluxes in desert ecosystems. When considering water resources, waste isolation, and contaminant transport, a thorough understanding of soil–plant–atmosphere interactions that control subsurface moisture fluxes is essential. Because water fluxes in arid environments are often small, an evaluation of subsurface processes requires a combination of adequate field measurements and numerical models (Phillips, 1994; Scanlon and Milly, 1994).

Previous studies showed that desert plants have a considerable effect on water flow processes in shallow desert soils (the upper 1 m) and thick unsaturated zones (10s of meters). One- to 12-yr field studies by Fischer (1992), Andraski (1997a), and Scanlon et al. (2003) showed a predominantly upward driving force for isothermal flow below the root zone of desert shrubs. The presence of native vegetation in arid and semiarid environments has been shown to eliminate deep drainage by limiting root-zone soil moisture accumulation (Gee et al., 1994). An 8-yr lysimeter study near the Nevada Test Site in southern Nevada indicated that evapotranspiration (ET) from vegetated soils reduced soil water storage at 10 times the rate of evaporation from bare soil alone (Scanlon et al., 2005a). This behavior was also reflected in numerical modeling studies by Walvoord et al. (2002, 2004) and Scanlon et al. (2003), which indicated that sparsely vegetated, thick vadose zones in the arid western United States are dominated by low water potentials and upward hydraulic gradients.

Thermally driven water vapor flow is an important process that can affect the water balance, water movement, and contaminant transport in arid climates as a result of dry soils and steep temperature gradients (Scanlon and Milly, 1994; Andraski et al., 2005; Saito et al., 2006). Field-based analytical models of contaminant movement through native, vegetated soil in the Amargosa Desert indicate that shallow vapor-phase tritium fluxes were upward and one to three orders of magnitude greater than liquid tritium fluxes (Andraski et al., 2005). Numerical models simulating water flow in the arid southwestern United States indicate that thermally driven vapor fluxes are dominant throughout most of the unsaturated zone (Scanlon et al., 2003; Walvoord et al., 2004). Shallow water flow simulations evaluating vegetative controls on water movement within natural and engineered soil in

arid regions typically focus on liquid water flow (Dong et al., 2003; Scanlon et al., 2005b; Young et al., 2006), however, neglecting the potential for water vapor transport. Yin et al. (2008) incorporated thermal vapor flow when simulating shallow paleowater fluxes, but their results documented total water fluxes rather than isothermal and thermal liquid water and water vapor components.

The objectives of this study were to evaluate vegetative and thermal vapor controls on soil water movement in an arid environment. The approach was to compare numerical simulations of coupled liquid water, water vapor, and heat flow in vegetated and unvegetated soil and to compare simulations with and without heat flow in vegetated soil. The model was accepted a priori as providing an accurate theoretical basis for exploring the processes incorporated therein; therefore no attempt was made to calibrate the model. Sensitivity analyses of leaf area index (LAI) and soil texture (sediment lithology) were used to understand the factors controlling water movement.

In contrast to previous modeling studies (Walvoord et al., 2002; Scanlon et al., 2003; Mayers et al., 2005), which applied a constant-head root sink at a fixed sub-root-zone depth to represent ET from a sparsely vegetated landscape, this study simulated the dynamic processes of evaporation, transpiration, and subsurface water flow in response to climate variability. The study used a heat-and-mass modeling approach similar to that of Yin et al. (2008), who evaluated changes in plant water uptake and Cl^- mass balance during the last 18,000 yr of reconstructed climate change. The current study executed a detailed analysis of the effects of heat flow on soil water movement in and beneath the root zone of vegetated soil during a recent 4.7-yr period. The analysis represents the first known attempt to differentiate the separate and combined influences of gas and liquid water movement as they interact with vegetation in the current arid environment. The study period included El Niño Southern Oscillation driven precipitation extremes, including the driest and third wettest years on record.

Methods

Field Site and Data Collection

The Amargosa Desert Research Site is located in the northern Mojave Desert, about 17 km south of Beatty, NV, and 20 km east of Death Valley National Park (Fig. 1). In the Basin and Range Province, the Amargosa Desert is bounded by Paleozoic rock and Tertiary volcanic rock mountains (Fischer, 1992). Surface soils are mapped as the Yermo (loamy-skeletal)–Arizo (sandy-skeletal) association (NRCS, 2004). Sediments are predominantly fluvial deposits consisting of several sand and gravel sequences (Nichols, 1987). Precipitation averages 112 mm yr^{-1} (1981–2005) and is highly variable from month to month and year to year (Johnson et al., 2007). Depth to the water table ranges from 85 to 115 m below the land surface (Fischer, 1992). The sparsely vegetated study site is dominated by creosote bush [*Larrea tridentata* (Sessé & Moc. ex DC.) Coville], an evergreen shrub (Smith et al., 1997). The root

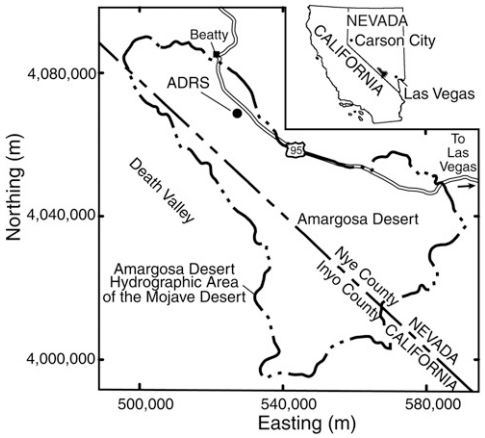

Fig. 1. Location map showing the Amargosa Desert Research Site (ADRS) near Beatty, NV. Base from USGS digital data (Universal Transverse Mercator projection, Zone 11, North American Datum of 1983).

system of creosote bush can exceed 4 m radially (Gile et al., 1998) and the rooting depth generally corresponds with the typical penetration depth of precipitation (<1 m; Andraski, 1997a). Water accumulation and deeper percolation are limited by plant transpiration, soil evaporation, and a capillary break formed by a gravelly layer underlying finer textured root-zone soil (Fischer, 1992; Andraski, 1997b).

Continuous 15-min eddy-covariance ET measurements were collected at the site from May 2002 to December 2005 (Johnson et al., 2007). Field ET data were collected about 200 m from the weather station where precipitation (collected at 1-m height) and solar radiation were measured. Daily ET rates represent the sum of 15-min data during a 24-h period.

Numerical Model

The HYDRUS-1D numerical code was used to simulate coupled liquid water, water vapor, and heat flow in variably saturated soil (Šimůnek et al., 2008). A one-dimensional modeling approach was accepted a priori as providing an acceptably accurate theoretical basis for initial exploration of the complex plant–soil–water interactions incorporated therein. Actual flow can be strongly three-dimensional, especially at shallow depths immediately after rainfall. Nevertheless, the one-dimensional approach was deemed appropriate because the modeled domain is relatively large (0–13 m). The one-dimensional results provide a foundation for future, high-resolution modeling of near-surface dynamics.

The extended version of Richards' equation, modified by Philip and de Vries (1957) to include temperature gradients in addition to pressure head gradients, was used to model interactions between liquid water, thermal (temperature-driven) vapor, isothermal (pressure-head-driven) vapor, and heat flow.

The governing equation for liquid and water vapor flow is

$$\frac{\partial \theta}{\partial t} = -\frac{\partial q_L}{\partial z} - \frac{\partial q_v}{\partial z} - S \quad [1]$$

where θ is the total volumetric water content (liquid and vapor) [$L^3\ L^{-3}$]; q_L and q_v are volumetric fluxes of liquid water and water vapor [$L\ T^{-1}$] (upward positive), respectively; t is time [T]; z is the spatial coordinate [L]; and S is a sink term representing root water uptake [T^{-1}]. The flux of liquid water, separated into isothermal, q_{Lh}, and thermal, q_{LT}, liquid fluxes is

$$q_L = q_{Lh} + q_{LT} = -K_{Lh}\left(\frac{\partial h}{\partial z} + 1\right) - K_{LT}\frac{\partial T}{\partial z} \quad [2]$$

where K_{Lh} [$L\ T^{-1}$] and K_{LT} [$L^2\ K^{-1}\ T^{-1}$] are the isothermal and thermal liquid hydraulic conductivities, respectively; h is pressure head [L]; and T is temperature [K]. The flux of water vapor, separated into isothermal, q_{vh}, and thermal, q_{vT}, vapor fluxes is

$$q_v = q_{vh} + q_{vT} = -K_{vh}\frac{\partial h}{\partial z} - K_{vT}\frac{\partial T}{\partial z} \quad [3]$$

where K_{vh} [$L\ T^{-1}$] and K_{vT} [$L^2\ K^{-1}\ T^{-1}$] are the isothermal and thermal vapor hydraulic conductivities, respectively, described in Šimůnek et al. (2008). The root water uptake function defined by Feddes et al. (1978) is

$$S(h) = \varepsilon(h) S_p \quad [4]$$

where $\varepsilon(h)$ is the root water uptake response function (dimensionless), controlled by the soil pressure head; and S_p is the potential water uptake rate [T^{-1}]. Plant root and soil matrix water fluxes are fully coupled and equations are solved simultaneously during the same time step. Heat transport by convection–dispersion for variably saturated media is

$$\frac{\partial C_p T}{\partial t} + L_0\frac{\partial \theta_v}{\partial t} = \frac{\partial}{\partial z}\left[\lambda(\theta)\frac{\partial T}{\partial z}\right] - C_w\frac{\partial q_L T}{\partial z} - C_v\frac{\partial q_v T}{\partial z} - L_0\frac{\partial q_v}{\partial z} - C_w S T \quad [5]$$

where λ(θ) is the apparent thermal conductivity of the soil [$J\ L^{-1}\ T^{-1}\ K^{-1}$]; C_p, C_w, and C_v are volumetric heat capacities [$J\ L^{-3}\ K^{-1}$] of the moist soil, liquid phase, and vapor phase, respectively; and L_0 is the volumetric latent heat of vaporization of liquid water [$J\ L^{-3}$].

The one-dimensional model domain extended to 13 m in the z direction and was divided into six lithologic intervals (Andraski and Jacobson, 2000). Although detailed investigation of the model results focused on the upper 2 m of the profile, the model domain extended to 13 m to minimize boundary effects on the numerical simulations. Model intervals were composed of loamy sand, gravelly coarse sand, and gravelly coarse sandy loam (Fig. 2A). Soil hydraulic and thermal properties are given in Table 1. Andraski and Jacobson (2000) suggested that the saturated isothermal liquid hydraulic conductivity value determined from laboratory measurements on disturbed samples (43.2 cm d^{-1}; Andraski, 1996) might underestimate the actual value. Thus, a preliminary sensitivity analysis (data not shown) was performed and evaluated by comparing simulated and previously measured pressure head trends (Andraski, 1997a) and simulated and concurrently measured water content trends (Johnson et al., 2007). The results confirmed that increasing the laboratory-measured value by one order of magnitude (432 cm d^{-1}) improved agreement between the simulated and observed trends.

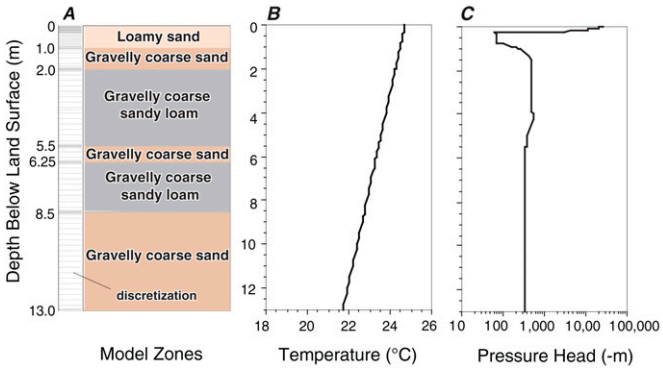

Fig. 2. (A) Model domain and initial conditions for (B) temperature and (C) pressure head. Model discretization increased at lithologic interval boundaries. The vegetated soil root-zone corresponds with the 0–1-m depth interval.

Creosote bush root water uptake parameters controlled by pressure head were inferred from field observations and associated measurements of root-zone water storage and water potentials (Andraski, 1997a, Fig. 9a). Maximum plant vigor and water uptake generally corresponded with periods when root-zone pressure heads were between −2000 and −7000 cm. Plant vigor generally decreased during early to mid-summer when pressure heads were between −7000 and −40,000 cm. The pressure head at which plants no longer transpire was assigned an approximate wilting point for creosote bush (−80,000 cm) based on Odening et al. (1974). The potential limiting transpiration rate parameters were based on HYDRUS-1D default values. The input water stress parameters for creosote bush for the Feddes et al. (1978) root water uptake model were: pressure head below which roots start to extract water, 0 cm; pressure head below which roots extract water at the maximum possible rate, −2000 cm; limiting pressure head values below which roots can no longer extract water at the maximum rate, higher limit −7000 cm, lower limit −40,000 cm (assuming a potential transpiration rate of 0.5 and 0.1 cm d^{-1}, respectively); pressure head below which root uptake ceases, −80,000 cm.

Boundary Conditions

The soil surface water-flow boundary was controlled by a time-variable atmospheric boundary condition including potential evaporation, potential transpiration, air temperature, and

Table 1. Input parameters describing the soil hydraulic (van Genuchten, 1980) and thermal (Campbell, 1985) properties of the model domain including residual (θ_r) and saturated (θ_s) water content; saturated hydraulic conductivity (K_s); curve-fitting parameters (α and n); volumetric heat capacities of the mineral soil (C_{hs}), water (C_w), and organic matter (C_o); volume fraction of organic matter (ϕ_o), solids (ϕ_n), clay (ϕ_c), quartz (ϕ_q), and other minerals (ϕ_m); and thermal longitudinal dispersivity (D_L).

Lithologic interval	Soil type	Hydraulic properties					Thermal properties								
							Volumetric heat capacity								
		θ_r†	θ_s†	K_s†	α‡	n‡	C_{hs}†	C_w§	C_o§	ϕ_o¶	ϕ_n§	ϕ_c§	ϕ_q§	ϕ_m§	D_L#
		—cm^3 cm^{-3}—		cm d^{-1}	cm^{-1}		— J cm^{-3} K^{-1} —								cm
1	loamy sand	0	0.29	432.0	0.036	1.29	2.32	4.18	2.5	0.0025	0.7	0.04	0.01	0.69	0.1
2, 4, 6	gravelly coarse sand	0	0.16	1036.8	7.150	1.18	2.28	4.18	2.5	0.0025	0.8	0.01	0.10	0.70	0.1
3, 5	gravelly coarse sandy loam	0	0.22	319.7	0.436	1.15	2.29	4.18	2.5	0	0.75	0.06	0.09	0.66	0.1

† Andraski and Jacobson (2000); K_s in Lithologic Interval 1 is one order of magnitude greater than the reference.
‡ Mayers et al. (2005).
§ Campbell (1985).
¶ California Soil Resource Lab.
# Hatch et al. (2006).

precipitation. Input values were based on daily data from the study site micrometeorological station (air temperature, solar radiation, and precipitation; Johnson et al., 2007). The lower water-flow boundary (13-m depth) was assumed to be controlled by gravity and was assigned a unit hydraulic gradient. The time-variable air temperature and constant bottom temperature (21.7°C; Fischer, 1992) were used for the upper and lower heat flow boundaries, respectively. The minimum pressure head (at residual water content) at the soil surface was assigned -5×10^4 m, the lower limit of allowable values in HYDRUS-1D. This value is greater than the oven-dry soil value (-9.2×10^4 m) used by Andraski (1996) but is similar to (i) the lowest shallow-soil (0–1-cm) field value (-4×10^4 m) determined from periodic water activity measurements made over several years and (ii) modeled soil surface values using the Rossi–Nimmo (-4.3×10^4 m) and Brooks–Corey (-3.6×10^4 m) retention functions (Andraski and Jacobson, 2000). Runoff at the study site was assumed negligible and the maximum thickness of the surface water layer was assigned 4 cm accordingly based on depression storage.

Potential evapotranspiration (PET), potential evaporation (PE), and potential transpiration (PT) were estimated and partitioned using methods similar to Kemp et al. (1997). The daily maximum PET (PET_{max}) [M L^{-2} T^{-1}] was computed as a simple function of measured daily maximum air temperature (T_a) [K] and solar radiation (S_{max}) [W L^{-2}] (Campbell, 1977, p. 141):

$$PET_{max} = \frac{[a(T_a + b)S_{max}]}{L_w} \quad [6]$$

where L_w is the latent heat of vaporization [J M^{-1}], and a = 0.025°C^{-1} and b = 4.6°C are constants. The daily PET was computed by integrating PET_{max} across the day (from 0 to π) assuming a sinusoidal course of energy and temperature (average daily PET = 2 PET_{max}/π), multiplying the average PET by the daylight hours, and converting units [L T^{-1}]. Daily PET was partitioned into PT for the canopy and PE for the soil surface using a Beer's law relation:

$$PT = PET[1 - \exp(kLAI)] \quad [7]$$

$$PE = PET \exp(-kLAI) \quad [8]$$

where k is the radiation extinction coefficient (dimensionless) and LAI is leaf area per unit ground area (dimensionless). The parameter k can vary with the sun angle and plant and leaf distribution; this study used k = 0.6 as suggested by Kemp et al. (1997).

The LAI input for the model was determined by extrapolating field-based literature estimates of LAI for a single creosote bush to the entire plant community. Maximum (1.9; Asner, 1998) and minimum (0.51; Gibson et. al., 2004) literature values for plant-scale LAI were averaged (1.2) and multiplied by the fractional cover of plants across the landscape. Fractional cover was determined from quarterly field measurements along four, 200-m-long transects using the line-transect method (Smith, 1974). Transect estimates of fractional cover within each quarter were averaged and interpolated between quarters. Fractional cover ranged from 0.04 to 0.10 and averaged 0.06. Although the measurements encompassed a mixed species plant community (Garcia et al., 2009), the model was parameterized as a single-species community because of creosote bush's relative dominance (on average, >80%) and evergreen character.

Initial Conditions

Initial conditions include temperature, pressure head, and root distribution profiles. The temperature profile (Fig. 2B) was estimated by interpolating between the average air temperature on Day Zero and the constant bottom boundary temperature of 21.7°C. The pressure head profile (Fig. 2C) was estimated using in situ field measurements made in vegetated soil under similar antecedent moisture conditions (Andraski, 1997a). Osmotic heads observed at the site (0 to −50 m; Fischer, 1992) were considered small relative to pressure heads and therefore were not considered in the numerical simulations. Vertical distribution of creosote bush roots (Table 2) was assumed to be similar to that for the Chihuahuan Desert (Kemp et al., 1997). Simulations began in May 2001.

Numerical Simulations

Individual 4.7-yr simulations that combined liquid water, water vapor, and heat flow were run with and without vegetation to evaluate vegetative controls on soil water movement. Simulations with and without vegetation also were run without heat flow (isothermal) to determine thermal vapor controls on water movement. Daily input and output data were used to evaluate temporal responses to climate variability. Numerical solutions were solved using a variable time discretization (10^{-6}–10^{-3} d) that was automatically adjusted based on the iterations necessary to reach convergence (Šimůnek et al., 2008). The 13-m soil profile was divided equally into 133 nodes with increasing discretization at surface–subsurface and material interfaces (Andraski and Jacobson, 2000). Field measurements indicated that a capillary break in the soil at the base of the root zone (the interface between loamy sand and gravelly coarse sand) probably impedes deeper liquid percolation. Therefore model sensitivity to the capillary break was tested for the aforementioned simulations by reducing the soil profile to a single lithologic material (loamy sand). A sensitivity analysis was also performed with variations in the LAI for the vegetated model with heat flow (described above) to improve understanding of biological factors controlling shallow water movement. Model sensitivity to the LAI, the primary surface component constraining simulated plant transpiration, was tested by varying its value for 100% cover from 0.51 (Gibson et al., 2004) to 1.9 (Asner, 1998). Simulations represent the LAI expressed on a plant-community basis.

Results and Discussion

Vegetated and Unvegetated Soil Simulations with Heat Flow

Precipitation and Air Temperature

Cumulative precipitation measured during the 4.7-yr study period (May 2001–December 2005) totaled 555 mm. Daily precipitation and daily average air temperature are shown in Fig. 3. Although 70% of the precipitation fell from October to April during the study, large monthly precipitation was measured in July 2001 (33 mm) and September 2005 (31 mm). Annual precipitation averaged 122 mm (2002–2005) and was 9% above the long-term average

Table 2. Input root distributions of creosote bush (*Larrea tridentata*) for the model domain.

Depth	Root distribution†
cm	
0–10	0
10–20	0.1
20–30	0.2
30–40	0.2
40–60	0.3
60–80	0.1
80–100	0.1

† Kemp et al. (1997).

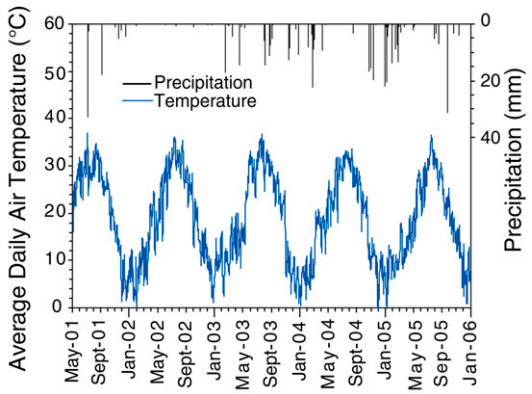

Fig. 3. Measured daily average air temperature and daily precipitation (Johnson et al., 2007).

(112 mm, 1981–2005; Johnson et al., 2007). The study captured La Niña (dry summer and winter, February 2002–February 2003) and El Niño (wet winter, November 2004–March 2005) events. The second year of the study, 2002, was the driest on record, with 4 mm of precipitation; 2005 was the third wettest year on record with 178 mm. Annual precipitation during 2004 and 2005 was 55 and 59% above average (174 and 178 mm, respectively). Air temperature averaged 18.3°C, with the warmest month (July) averaging 31.7°C and the coldest month (December) averaging 6.4°C (Johnson et al., 2007).

Water Storage

Major simulated changes in water storage were limited to the root zone (upper 1 m). The largest increases occurred during March 2004, October 2004, January 2005, and September 2005 in response to large precipitation pulses (20–31 mm d^{-1}) (Fig. 4). Root-zone water storage for vegetated soil decreased to a "baseline" value of about 25 mm by the end of each summer and showed little long-term change during the study. In contrast, storage for bare soil showed a long-term increase of about 39 mm (86%) between May 2001 and January 2006. Rates of moisture depletion after precipitation were also greatest for the vegetated soil. For example, during March to June 2005, vegetated soil values decreased

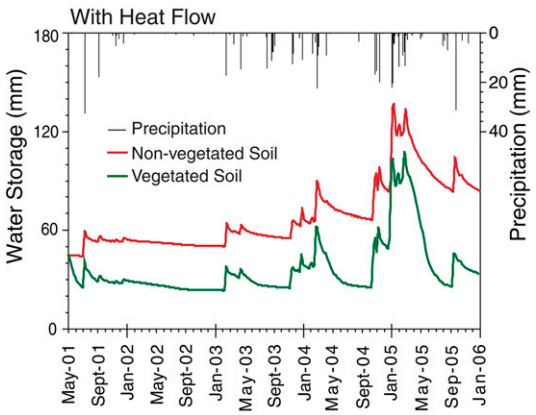

Fig. 4. Simulated root-zone (0–1-m depth) water storage for vegetated and unvegetated soil and measured daily precipitation (Johnson et al., 2007).

twice as fast as those for unvegetated soil and reached the annual minimum within about 6 mo (Fig. 4).

Pressure Head

Simulated pressure heads for vegetated and unvegetated soil are shown with precipitation in Fig. 5A–5B. Pressure heads within the root zone of the vegetated soil increased rapidly (up to 80 m in 1 d at the 25-cm depth, November 2004; Fig. 5A) in response to precipitation. These large increases were followed by large decreases at rates of up to 10 m d^{-1} (25- and 50-cm depths, spring 2005). For the unvegetated soil, these wetting and drying cycles were considerably more muted, as pressure heads at depths above and in the shallow gravelly layer (1–2 m) all showed long-term increases (Fig. 5B). Bare-soil pressure heads at the 25-, 50-, 101-, and 150-cm depths increased by 66, 75, 94, and 35%, respectively, during the simulation period.

Pressure head gradients in the root zone of the vegetated soil typically provided a downward driving force for isothermal flow during cooler, wetter months and an upward driving force during warmer, drier months (Fig. 3 and 5A). Gravitational heads were small (0 to −13 m) with respect to pressure heads and effects on isothermal flow were considered negligible. Pressure head gradients in the unvegetated soil followed similar trends; however, accumulating moisture dampened these gradients as the simulation time progressed (Fig. 5B).

Simulated pressure heads in the sub-root-zone shallow gravel (Fig. 5A and 5B; 101- and 150-cm depths) oscillated seasonally. For the vegetated soil, the driving force for isothermal flow between the 101- and 150-cm depths was primarily upward, with the exception of the spring of 2005 El Niño event, when precipitation penetrated below the root zone, inverting the pressure head gradient and isothermal flow direction (Fig. 5A). For the unvegetated soil, pressure heads throughout the shallow gravelly layer decreased with increasing depth, providing a downward driving force for flow.

Below the shallow gravelly layer (>200-cm depth), variations in pressure heads for the vegetated and unvegetated soils were similar, reflective of initial conditions (Fig. 2C), and showed no long-term change or response to El Niño precipitation. Pressure head gradients showed a persistent upward driving force for isothermal flow between the 2.4- and 13-m depths for the unvegetated soil and between the 2- and 13-m depths for the vegetated soil (data not shown). Vegetated-soil pressure heads at and below 2.5 m increased with depth and showed small seasonal fluctuations, averaging −492 ± 9, −351 ± 0.2, and −330 ± 0.3 m at the 2.5-, 7-, and 12-m depths, respectively. Temperatures at these depths averaged 19.8 ± 2.3, 20.6 ± 0.3, and 21.5 ± 0.03°C, respectively.

Simulated pressure heads for the vegetated and unvegetated soils were generally consistent with a previous field study where water potentials (driven primarily by pressure head) were measured continuously for 5 yr using thermocouple psychrometers (Andraski, 1997a). For example, within the root zone of the vegetated

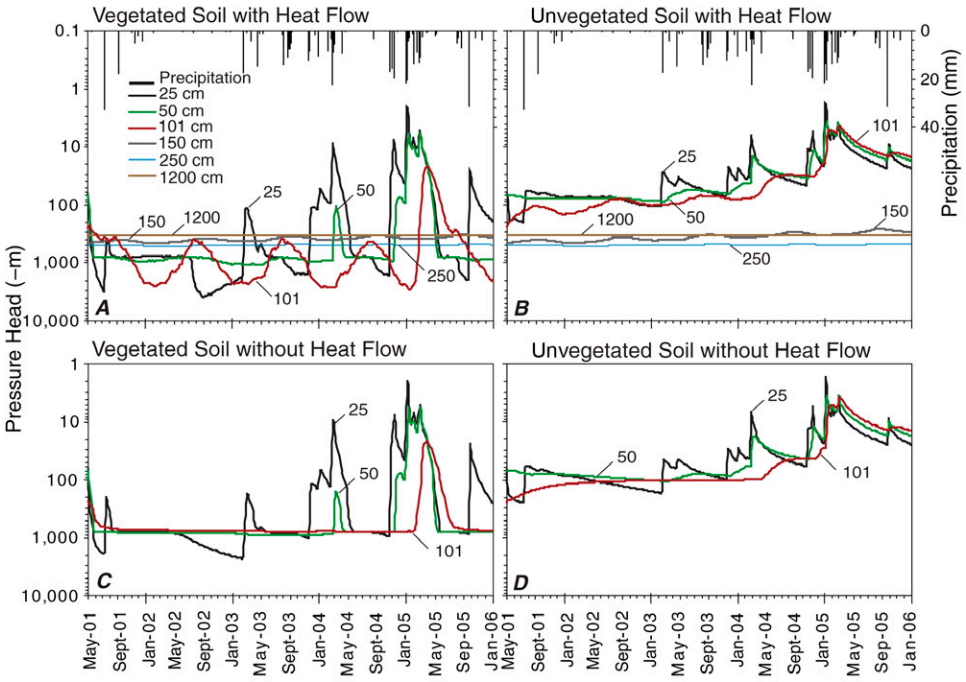

Fig. 5. Simulated pressure heads for (A) vegetated and (B) unvegetated soil with heat flow and (C) vegetated and (D) unvegetated soil without heat flow and measured daily precipitation (Johnson et al., 2007). The root zone and shallow gravel extend from 0 to 1 and 1 to 2 m, respectively.

soil, simulated and measured values both showed rapid increases above −100 m following precipitation and often dipped below the range of psychrometer measurement (less than −800 m) during soil drying. For the unvegetated soil, simulated and measured values near 50 and 75 cm below the land surface remained elevated (more than −100 m). In addition, the simulated seasonal oscillations in heads for the sub-root-zone gravelly layer were consistent with field data collected at both vegetated and unvegetated soil sites.

Evapotranspiration

A comparison between cumulative simulated unvegetated soil evaporation and vegetated soil ET is shown in Fig. 6 along with the measured precipitation. Total evaporation for the unvegetated soil was 42 mm less than precipitation and averaged 114 mm annually (2002–2005). In contrast, simulated cumulative ET for the vegetated soil was about 11 mm greater than the cumulative precipitation and averaged 120 mm annually (2002–2005). The 11-mm difference was attributed to the initial (May 2001) evapotranspirative removal of antecedent moisture from storage. Greater cumulative ET than precipitation indicates that the soil–plant–atmosphere system removed water from storage and inhibited long-term accumulation of infiltrating precipitation. The greatest monthly ET for the vegetated and unvegetated soils was simulated for February 2005 (45 and 48 mm, respectively), while the lowest was simulated for October 2003 (0 mm).

Total cumulative ET for the vegetated soil was 566 mm (Fig. 6), of which 424 mm was attributed to evaporation and 142 mm to transpiration. Therefore, the total simulated evaporation/transpiration (E/T) flux ratio for the vegetated soil was 3:1. This ratio is similar to the average ratio determined by a 2.4-yr field study at the Amargosa Desert Research Site where eddy covariance and chamber-based bare-soil evaporation measurements were combined to estimate continuous ET, bare-soil E, and plant T (Garcia et al., 2009).

A qualitative comparison between daily simulated vegetated-soil ET and daily field ET reported by Johnson et al. (2007) for 1 May 2002 through 31 Dec. 2005 is shown in Fig. 7. Simulated and field-determined (eddy-covariance) ET followed similar temporal trends, with greater fluxes following precipitation and minimal fluxes during dry periods. As illustrated in the Fig. 7 inset, however, simulated ET responses to precipitation were often greater in magnitude but shorter in duration than field ET responses. In contrast to the spiky nature of the simulated ET time series, the field ET record generally showed more gradual, exponential declines following precipitation. Recognizing the synthetic nature of simulated ET fluxes, such differences are not surprising, but they do highlight potential uncertainties in the multiyear simulations of water and heat flow. For example, the use of a simple PET model (Eq. [6]) might have led to artificially high simulated ET when water was readily available immediately following precipitation. Also, inaccuracies in the prescribed (but not optimized) soil water retention function and soil hydraulic properties could have

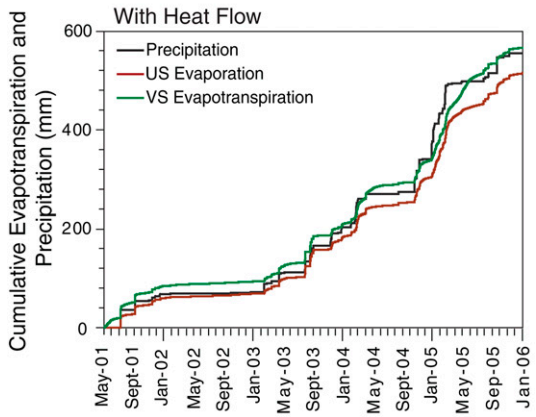

Fig. 6. Cumulative simulated unvegetated soil (US) evaporation and vegetated soil (VS) evapotranspiration, and measured precipitation (Johnson et al., 2007).

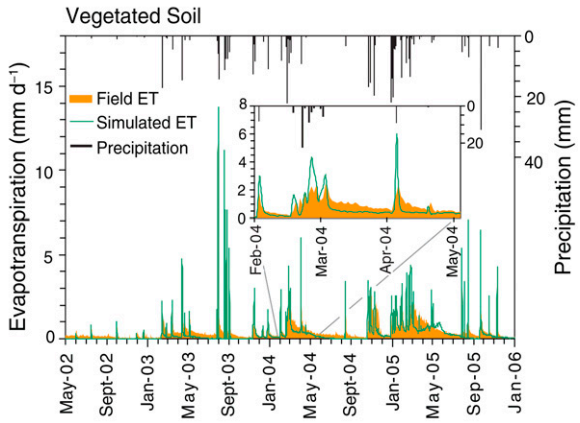

Fig. 7. General trends in simulated vegetated soil evapotranspiration and field-determined eddy-covariance evapotranspiration with measured daily precipitation (Johnson et al., 2007).

affected the simulated amount of water lost to the atmosphere by evaporation as well as the amount of infiltration.

Water Movement

Simulated fluxes of total water, isothermal and thermal liquid water, and isothermal and thermal water vapor within and just below the root zone of the vegetated and unvegetated soils are shown in Fig. 8. Although absolute flux values are highly uncertain due to the uncertainty of hydraulic properties (both isothermal and thermal), comparisons within and between simulations provide insight into the physical processes driving water movement. Root-zone total water fluxes for vegetated and unvegetated soil followed similar trends at all depths throughout the study, but downward total water fluxes at the 50-cm depth following precipitation in February 2004 and October to December 2004 were typically greater for the unvegetated soil (Fig. 8A–8B). For example, following February 2004 precipitation, the peak total water flux at the 50-cm depth for the unvegetated soil was an order of magnitude greater than for the vegetated soil (−0.1 and −0.03 mm d^{-1}, respectively).

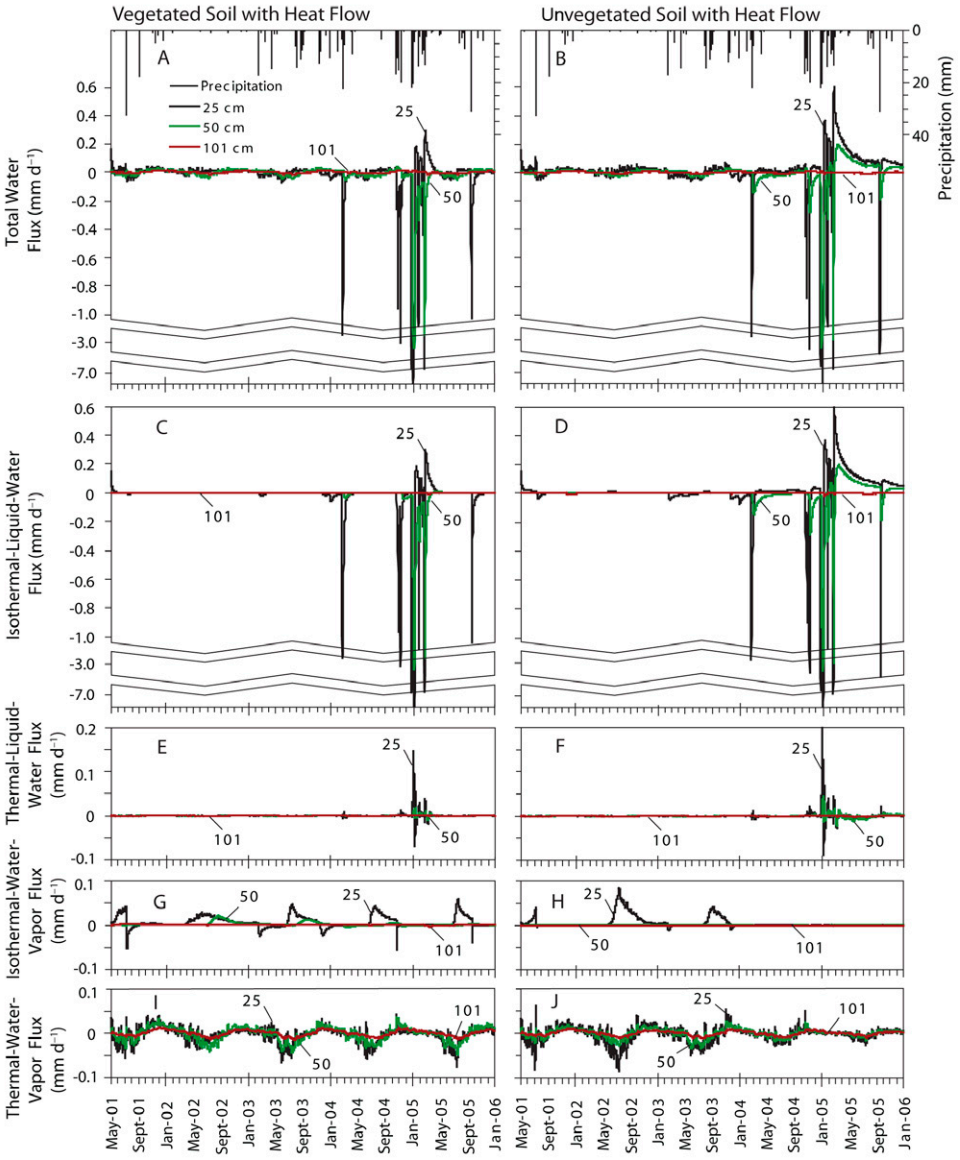

Fig. 8. Simulated total water and isothermal and thermal liquid water and water vapor fluxes for (A, C, E, G, I) vegetated and (B, D, F, H, J) unvegetated soil with measured daily precipitation (Johnson et al., 2007). The root zone extends from 0- to 1-m depth. Sign convention is that downward fluxes are negative. Scales for A to D differ from E to F.

on average at the 101-cm depth) (Fig. 8C–8F). In response to the 2004–2005 El Niño, however, a small (10^{-3} mm d^{-1}) but sustained downward isothermal liquid flux led to moisture penetration and increased water content (0.024 m^3 m^{-3}) just below the capillary break at 100 cm. During the following summer, ET of root-zone water fostered upward isothermal liquid fluxes that removed this deeper penetrating liquid. This was also shown following the La Niña event (February 2002–February 2003) when extended root-zone drying caused a shift in liquid water fluxes at the 150-cm depth from downward to upward. In contrast, in unvegetated soil, isothermal liquid fluxes throughout the gravelly layer were consistently downward during the study.

Although the isothermal liquid water flux dominated downward water movement during short time periods, total moisture transport during the 4.7-yr simulation period was dominated by thermal water vapor fluxes (Fig. 8). For example, at the 50-cm depth, the thermal vapor flux was dominant nearly 90 and 60% of the time and averaged -10^{-3} and -10^{-4} mm d^{-1} for vegetated and unvegetated soil, respectively. Within the sub-root-zone gravelly layer, thermal vapor flux directions varied seasonally and magnitudes averaged $\sim 10^{-4}$ mm d^{-1} (data not shown); these fluxes were dominant nearly 100% of the time.

The relatively large downward total fluxes following fall to spring precipitation in 2004 and 2005 were dominated by isothermal liquid water movement through the root zone, during which time thermally driven liquid water fluxes were comparatively negligible (Fig. 8A–8B vs. 8C–8D). Isothermal liquid fluxes for unvegetated soil were typically greater than those for vegetated soil and often penetrated deeper as a result of moisture accumulation and associated increases in isothermal liquid conductivities.

Just below the capillary break at the root zone–gravelly layer interface (100-cm depth), liquid water fluxes for the vegetated soil trended upward and downward seasonally but were predominantly negligible with respect to root-zone fluxes (10^{-5} mm d^{-1}

As shallow moisture accumulated with simulation time for the unvegetated soil, water vapor fluxes were dampened with respect to the vegetated soil. For example, although similar in magnitude near the start of the simulation, isothermal water vapor fluxes at the 25-cm depth were, on average, two orders of magnitude greater than those for the unvegetated soil beyond winter 2004 (Fig. 8G–8H). A similar trend was shown for thermal water vapor fluxes at 25 cm; although initially similar, fluxes for the vegetated soil were twice as great as those for the unvegetated soil near the end of the simulation (Fig. 8I–8J). At and below 50 cm, thermal water vapor fluxes for the vegetated soil were, on average, about 50% greater than the unvegetated fluxes.

Simulated fluxes beneath the root zone of vegetated and unvegetated soil were consistent with previous studies where fluxes were computed analytically using field data. For example, for vegetated soil, the magnitude of fluxes calculated by Andraski (1997a) for the shallow gravelly layer were about 10^{-11} to 10^{-10} mm d^{-1} for isothermal liquid water, 10^{-5} mm d^{-1} for thermal vapor, and about 10^{-7} mm d^{-1} for isothermal vapor during September 1990 and September 1992. Simulated fluxes for the month of September (2001–2005) were about 10^{-11} to 10^{-10} mm d^{-1} for isothermal liquid water, 10^{-4} to 10^{-3} mm d^{-1} for thermal vapor, and 10^{-6} to 10^{-5} mm d^{-1} for isothermal vapor. In a previous study, Fischer (1992) computed average monthly thermal vapor fluxes ranging from 10^{-4} to 10^{-1} mm d^{-1} in the gravelly layer. Simulated average monthly thermal vapor fluxes for vegetated soil also ranged from 10^{-4} to 10^{-1} mm d^{-1} in the gravelly layer.

Cumulative total water fluxes for vegetated and unvegetated soil indicate that water movement below the root zone is minimal under current climatic conditions. Cumulative total water flux profiles for vegetated and unvegetated soil are shown in Fig. 9. The cumulative total water flux in the vegetated soil was upward but minimal (0.93 mm during 4.7 yr at the 101-cm depth, corresponding to a flux of 0.2 mm yr^{-1}). In the unvegetated soil, the total water flux was downward to a depth of 150 cm, with a net flux of −1.3 mm during 4.7 yr at the 101-cm depth (corresponding to −0.3 mm yr^{-1}). Previous field studies (Fischer, 1992; Andraski, 1997b) suggested that a capillary break in the soil at the base of the root zone (the interface between loamy sand and gravelly coarse sand) might partly explain the lack of deeper water penetration. Additional simulations for vegetated and unvegetated soil using a homogeneous soil profile (loamy sand) indicated that the capillary break had little effect on cumulative total water fluxes for the vegetated case but relatively large effects for the unvegetated case (Fig. 9). The cumulative water flux for the vegetated soil at the 101-cm depth increased by 0.5 mm in the absence of layering (Fig. 9A), whereas the corresponding unvegetated soil flux increased by 34 mm (Fig. 9B).

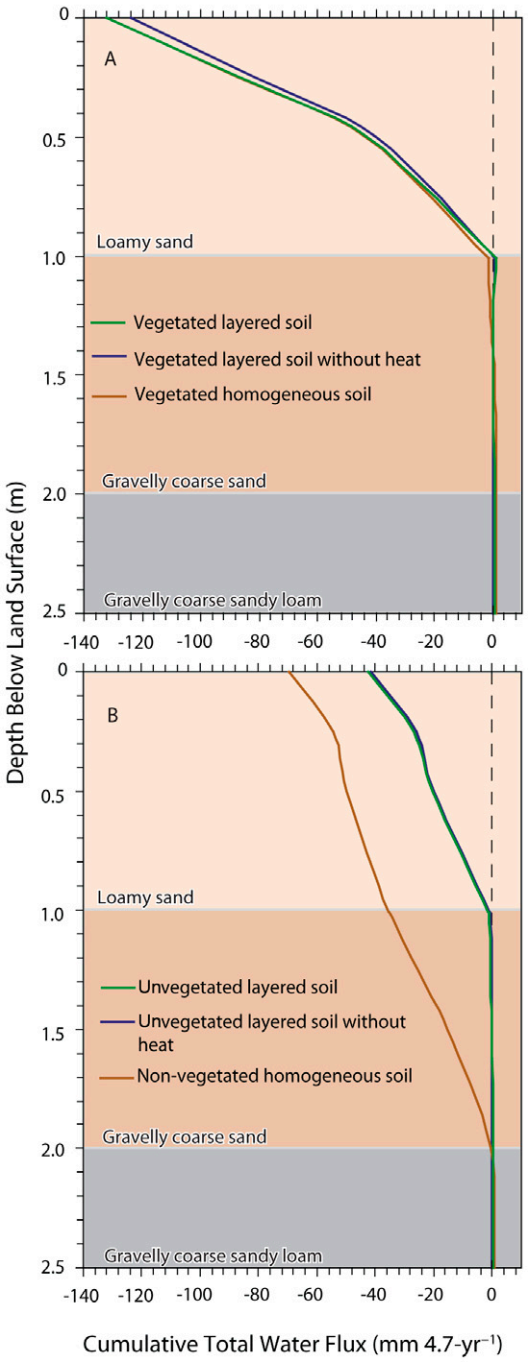

Fig. 9. Simulated cumulative total subsurface water flux during a 4.7-yr period for (A) vegetated and (B) unvegetated soil. Fluxes are for simulations with heat flow in layered and homogeneous soil and without heat flow in layered soil. Sign convention is that downward fluxes are negative.

Thermal Water Vapor Contributions to Water Movement

Water storage simulated with and without heat flow is shown in Fig. 10. For the vegetated soil, peak water storage values following precipitation were similar for simulations with and without heat. Depletion of accumulated water was consistently greater when heat flow was included, however, and this resulted in late summer to early fall storage values that were 0.5 to 2 mm less than those for the no-heat simulation (Fig. 10A). These differences are linked to plant water uptake during mid- to late summer (discussed below). For unvegetated soil, the no-heat-flow simulation produced storage values that were up to 5 mm greater than those with heat flow (Fig. 10B). Thermal vapor flow probably redistributed the available moisture below the evaporation extinction depth (about 50 cm), allowing condensation and greater moisture accumulation.

Pressure heads simulated without heat flow for vegetated and unvegetated soil are shown in Fig. 5C–5D. Within and just below the root zone, pressure heads for the simulation without heat flow showed no seasonal fluctuation (Fig. 5C), whereas simulations with heat flow (Fig. 5A) and field measurements (Andraski, 1997a)

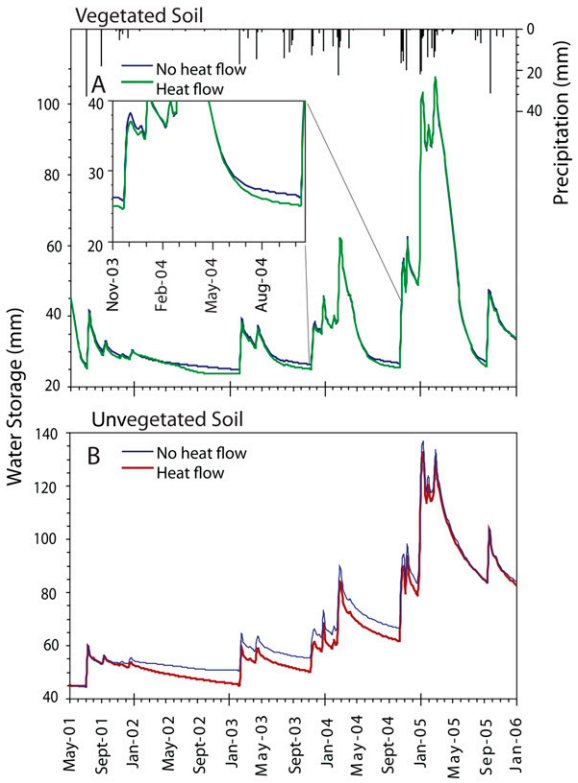

Fig. 10. Simulated root-zone (0–1-m depth) water storage with and without heat flow for (A) vegetated and (B) unvegetated soil and measured daily precipitation (Johnson et al., 2007). Inset shows an example of differences in storage during winter and summer months.

both showed substantial seasonal changes. Thus, the simulation without heat flow did not capture the dynamics of pressure head changes that can affect the rates and directions of water flow. For unvegetated soil, annual and multiyear pressure head trends for the no-heat-flow simulation (Fig. 5D) were similar to those with heat flow (Fig. 5B) as moisture accumulated with time.

Total root-zone water fluxes following precipitation were similar for simulations without and with heat because the isothermal liquid flux was predominant (see, for example, winter 2004–2005 results in Fig. 8A and 8C). In contrast, during dry periods total fluxes for the simulation without heat (data not shown) were primarily upward and driven by isothermal vapor flow while those simulated with heat trended upward and downward seasonally with a combination of thermal and isothermal vapor flow (Fig. 8A). At the 25-cm depth, isothermal and thermal vapor flux magnitudes were similar, thus the total water flux was similar for simulations with and without heat flow. At the 50-cm depth, however, the exclusion of heat flow during dry periods typically decreased total water fluxes and isothermal vapor fluxes by an order of magnitude.

As with the lack of seasonal dynamics observed for pressure heads in simulations without heat flow, isothermal liquid fluxes just below the capillary break (i.e., the 101-cm depth) were essentially constant and upward (10^{-6} mm d^{-1} on average), whereas those simulated with heat flow trended upward during warmer months and downward during cooler months (10^{-6} mm d^{-1} on average). Below the 101-cm depth (data not shown), the magnitude of the total water flux for the simulations without heat was, on average, one to three orders of magnitude less than the simulation with heat.

Root water uptake simulated with and without heat flow is shown in Fig. 11. The simulation with heat flow indicated that shallow root water uptake (25–30-cm depth interval) can occur during droughts and often persisted for a longer period than for the simulation without heat flow. An even more dramatic difference between root water uptake for the simulations with and without heat flow is illustrated by the results for the 95- to 100-cm depth interval. For example, the simulation with heat flow showed three notable increases in uptake at this interval that peaked in August of 2002, 2003, and 2004 (Fig. 11A), but no such increases were simulated without heat flow (Fig. 11B). The periods of increased uptake for the simulation with heat (accumulating to ~1 mm on average) corresponded directly with the previously noted difference in water storage and the seasonal increase in pressure head to peak values at the 101-cm depth (Fig. 5A). A combination of downward thermal vapor fluxes within the root zone and upward liquid water fluxes from just below the root zone probably led to the amassing of moisture at depth (95–100-cm depths) and the increased availability of liquid water for plant uptake. This combination of processes is similar to a sand column experiment simulated by Sakai et al. (2009), where water vapor driven downward by temperature

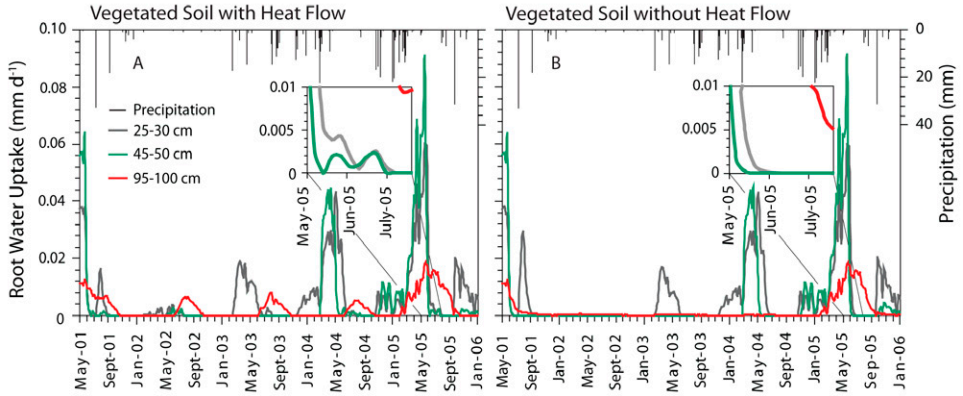

Fig. 11. Root water uptake for selected depth intervals simulated (A) with and (B) without heat flow in vegetated soil with measured daily precipitation (Johnson et al., 2007).

gradients condensed at the cooler base of the column and pressure head gradients subsequently drove liquid water upward. Based on current simulation results, we hypothesize that such a process could provide a small but noteworthy source of water for plants at the driest time of the year; however, field or laboratory measurements will be necessary to test this hypothesis. If verified, this previously unrecognized source of moisture could have ecohydrological implications for desert plant communities.

Total cumulative ET for the vegetated soil was similar for the simulations with and without heat flow (data not shown). The proportions of ET (E/T ratio) attributed to plant transpiration varied by 2% between simulations with and without heat. While the totals were similar, differences that did occur were concentrated during the summer months when increased root water uptake was simulated with heat flow. For the unvegetated soil, cumulative E simulated without heat flow was about 1 mm greater than with heat flow.

Model Sensitivity to Leaf Area Index

Model sensitivity to the LAI, the primary aboveground parameter constraining simulated plant transpiration, was tested by varying the LAI base value (i.e., 1.2 × cover) from 0.4 LAI (0.51 × cover) to 1.6 LAI (1.9 × cover). A comparison of root-zone water storage for variations in the LAI is shown in Fig. 12. Relative trends in water storage were similar for all LAI values; however, the rate and amount of moisture depletion were least for 0.4 LAI (e.g., March–Sept. 2005; Fig. 12). Despite varying depletion rates, predictions from the base-case and 1.6 LAI simulations reached similar minimum storage values (25 mm) during September of each year (Fig. 4 and 12, respectively). In contrast, minimum storage values for the 0.4 LAI simulation typically exceeded those for other simulations by 1 to 10 mm.

The effects of varying the LAI on the simulated cumulative ET time series are shown in Fig. 13. The total cumulative ET for the 4.7-yr simulations was 553 mm for 0.4 LAI, 566 mm for the base case, and 568 mm for 1.6 LAI; precipitation totaled 555 mm. The large difference between the 0.4 LAI and the base-case LAI reflects differences in storage and accumulating moisture. As anticipated, the cumulative proportion of ET attributed to transpiration increased with increasing LAI: the E/T flux ratios were 79:21 for 0.4 LAI, 75:25 for the base case, and 73:27 for 1.6 LAI.

Summary statistics comparing simulated daily ET time series for varying LAI values indicate that LAI variability had a minimal affect on the daily ET (Table 3). The mean difference between the daily simulated ET for the base LAI and sensitivity values ranged from 0.0007 to −0.0001 mm d^{-1} for 0.4 LAI and 1.6 LAI, respectively. The 1.6 LAI value was the most correlated ($r = 0.996$, $P < 0.0001$, Table 3) with the base LAI and showed the lowest maximum absolute difference (0.048 mm d^{-1}). Variations in LAI did little to improve comparisons between the simulated and field-determined ET shown in Fig. 7.

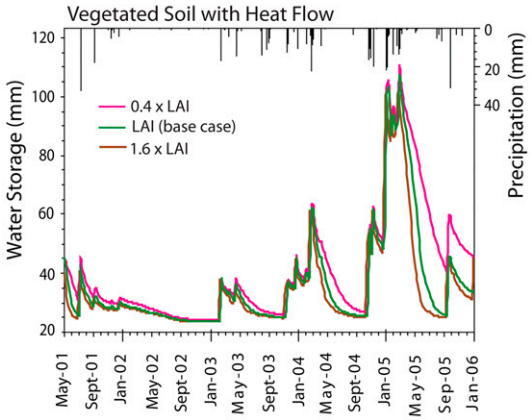

Fig. 12. Simulated root-zone (0–1-m depth) water storage showing the effects of varying leaf area index (LAI) values about the base-case values for simulations in vegetated soil with measured daily precipitation (Johnson et al., 2007).

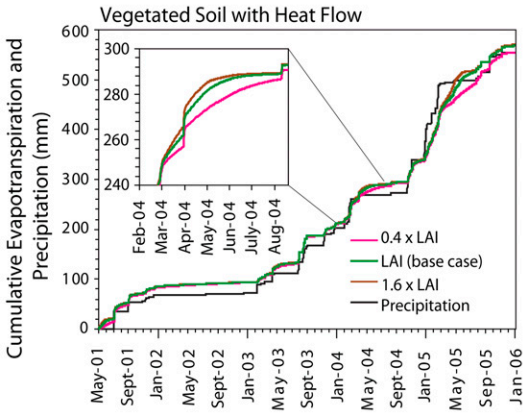

Fig. 13. Cumulative simulated evapotranspiration showing the effects of varying leaf area index (LAI) values about the base-case value for simulations in vegetated soil with heat flow. Inset shows an example of the differences in the rate of evapotranspiration increases during spring and summer.

Conclusions

Plant and temperature contributions to dynamic water movement in desert soils were investigated using a comprehensive model that coupled isothermal liquid, isothermal vapor, and nonisothermal liquid and vapor flow. Plant uptake of root-zone (upper 1 m) moisture triggered an upward driving force for isothermal flow. Similar to field measurements (Andraski, 1997a), nonisothermal simulations of large rainfall related increases in pressure head and water storage within the root zone of vegetated soil were followed by similarly large decreases. Negligible changes in water content within the underlying coarse gravel indicate that infiltrating precipitation was effectively removed by ET on an annual basis. For unvegetated soil, increasing root-zone water storage and pressure heads within and below the root zone during the 4.7-yr study indicated long-term moisture accumulation. Continued mois-

Table 3. Summary statistics for comparisons between simulated daily evapotranspiration for vegetated soil (VS) using the base leaf area index (LAI) and sensitivity values.

Simulation	LAI	Evapotranspiration					
					Difference†		
		r^2	RMSE	Pearson's r	Median	Mean	Max. absolute
					mm d^{-1}		
VS with heat	0.4 × LAI	0.990	0.009	0.995 (<0.0001)	0.000	0.0007	0.054
VS with heat	1.6 × LAI	0.993	0.008	0.996 (<0.0001)	0.000	−0.0001	0.048

† Base LAI minus LAI sensitivity values.

ture accumulation, in turn, created a persistent driving force for downward isothermal flow.

Similar to previous studies (Fischer, 1992; Andraski, 1997a), thermal vapor flow in the vegetated soil was the dominant mechanism for water movement in the root zone and upper portion of the underlying gravelly layer during warm periods and cool dry periods and at all times below this gravelly layer. Exclusion of thermal vapor flow from vegetated soil limited the extent of shallow soil drying and reduced pressure head gradients, ultimately restricting the magnitude of isothermal flow. Total water fluxes predicted without heat transport were, on average, an order of magnitude less than predictions with heat transport in the mid- to lower root zone and one to three orders of magnitude less below the root zone.

Negligible vapor movement in simulations without heat transport minimized redistribution of moisture within the root zone. In contrast, simulations with heat transport altered the temperature and pressure head gradients, providing a mechanism for moisture redistribution within and just below the root zone. Similar to a previous study where water vapor circulation and condensation was simulated in a sand column (Sakai et al., 2009), this vapor circulation–condensation process supplied additional moisture for root water uptake near the base of the root zone during the summer of each year. Redistribution of moisture during the summer months also triggered a notable difference in the cumulative proportion of ET attributed to transpiration, e.g., E/T ratios of 75:25 for simulations with heat flow and 77:23 without. Thermally driven vapor condensation during the driest part of the year might be an important source of water for plants, although field and laboratory measurements are necessary to test this hypothesis.

Cumulative total water fluxes for vegetated and unvegetated soil simulations with heat flow indicated that moisture penetration below the root zone and the capillary break in the soil was negligible. Additional simulations using a homogeneous soil profile indicate, however, that while the capillary break in the soil had little effect on the vegetated results, it had a large influence on the unvegetated results. The cumulative amount of moisture penetrating below the root zone of the unvegetated soil increased from about 1 mm with a capillary break to 35 mm without. In an environment with similarly stratified soils and sediments, disturbance of such capillary breaks could have large implications for long-term drainage.

Simulation results provide a greater understanding of soil–plant–atmosphere interactions that control the shallow moisture flux regime in arid environments. To our knowledge, this study is the first to delineate the temporal effects of heat flow on soil water movement in a vegetated soil. The inclusion of vegetation along with coupled isothermal and nonisothermal water flow identified interactions that have potential ecohydrologic implications for desert environments. In particular, the presence of plants and heat transport were shown to have notable effects in limiting downward sub-root-zone water movement and in supplementing the delivery of moisture to plant roots during the driest parts of the year.

Acknowledgments

We gratefully acknowledge Michael J. Fayer, Edwin P. Weeks, and anonymous reviewers for helpful comments on the manuscript. Support for this work was provided through the U.S. Geological Survey's Toxic Substances Hydrology, National Research, and Groundwater Resources programs.

References

Andraski, B.J. 1996. Properties and variability of soil and trench fill at an arid waste-burial site. Soil Sci. Soc. Am. J. 60:54–66. doi:10.2136/sssaj1996.03615995006000010011x

Andraski, B.J. 1997a. Soil-water movement under natural-site and waste-site conditions– A multiple-year field study in the Mojave Desert, Nevada. Water Resour. Res. 33:1901–1916. doi:10.1029/97WR01502

Andraski, B.J. 1997b. Test-trench studies in the Amargosa Desert, southern Nevada: Results and application of information to landfill covers in arid environments. *In* Landfill capping in the semi-arid West: Problems, perspectives, and solutions. Proc. Conf., Grand Teton National Park, WY. 21–22 May 1997. Environ. Sci. and Res. Foundation, Idaho Falls, ID.

Andraski, B.J., and E.A. Jacobson. 2000. Testing a full-range soil-water retention function in modeling water potential and temperature. Water Resour. Res. 36:3081–3089. doi:10.1029/2000WR900193

Andraski, B.J., D.A. Stonestrom, R.L. Michel, K.J. Halford, and J.C. Radyk. 2005. Plant-based plume-scale mapping of tritium contamination in desert soils. Vadose Zone J. 4:819–827.

Asner, G.P. 1998. Biophysical and biochemical sources of variability in canopy reflectance. Remote Sens. Environ. 64:234–253. doi:10.1016/S0034-4257(98)00014-5

Campbell, G.S. 1977. An introduction to environmental biophysics. Springer-Verlag, Berlin.

Campbell, G.S. 1985. Soil physics with BASIC: Transport models for soil–plant systems. Elsevier, New York.

Dong, W., Y. Zhongbo, and D. Weber. 2003. Simulations on soil water variations in arid regions. J. Hydrol. 275:162–181. doi:10.1016/S0022-1694(03)00041-6

Feddes, R.A., P.J. Kowalik, and H. Zarandy. 1978. Simulation of field water use and crop yield. John Wiley & Sons, New York.

Fischer, J.M. 1992. Sediment properties and water movement through shallow unsaturated alluvium at an arid site for disposal of low-level radioactive waste near Beatty, Nye County, Nevada. Water Resour. Invest. Rep. 92-4032. USGS, Denver, CO.

Garcia, C.A., B.J. Andraski, C.A. Cooper, D.A. Stonestrom, M.J. Johnson, R.L. Michel, and S.W. Wheatcraft. 2009. Transport of tritium contamination to the atmosphere in an arid environment. Vadose Zone J. 8:450–461.

Gee, G.W., P.J. Wierenga, B.J. Andraski, M.H. Young, M.J. Fayer, and M.L. Rockhold. 1994. Variations in water balance and recharge potential at

three western desert sites. Soil Sci. Soc. Am. J. 58:63–72. doi:10.2136/sssaj1994.03615995005800010009x

Gibson, A.C., M.R. Sharifi, and P.W. Rundel. 2004. Resprout characteristics of creosote bush (*Larrea tridentata*) when subjected to repeated vehicle damage. J. Arid Environ. 57:411–429. doi:10.1016/S0140-1963(03)00120-4

Gile, L.H., R.P. Gibbens, and J.M. Lenz. 1998. Soil-induced variability in root systems of creosotebush (*Larrea tridentata*) and tarbush (*Flourensia cernua*). J. Arid Environ. 39:57–78. doi:10.1006/jare.1998.0377

Hatch, C.E., A.T. Fisher, J.S. Revenaugh, J. Constantz, and C. Ruehl. 2006. Quantifying surface water–groundwater interactions using time series analysis of streambed thermal records: Method development. Water Resour. Res. 42:W10410. doi:10.1029/2005WR004787

Johnson, M.J., C.J. Mayers, C.A. Garcia, and B.J. Andraski. 2007. Selected micrometeorological, soil-moisture, and evapotranspiration data at Amargosa Desert Research Site in Nye County near Beatty, Nevada, 2001–2005. Data Ser. 284. Available at pubs.usgs.gov/ds/2007/284/ (accessed 26 Oct. 2007; verified 6 Feb. 2011). USGS, Reston, VA.

Kemp, P.R., J.F. Reynolds, Y. Pachepsky, and J.L. Chen. 1997. A comparative modeling study of soil water dynamics in a desert ecosystem. Water Resour. Res. 33:73–90. doi:10.1029/96WR03015

Mayers, C.J., B.J. Andraski, C.A. Cooper, S.W. Wheatcraft, D.A. Stonestrom, and R.L. Michel. 2005. Modeling tritium transport through a deep unsaturated zone in an arid environment. Vadose Zone J. 4:967–976.

Nichols, W.D. 1987. Geohydrology of the unsaturated zone at the burial site for low-level radioactive waste near Beatty, Nye County, Nevada. Water-Supp. Pap. 2312. USGS, Denver, CO.

NRCS. 2004. Soil Survey Geographic (SSURGO) database for Nye County, Nevada, southwest part. Available at SoilDataMart.nrcs.usda.gov/ (accessed 15 Mar. 2007; verified 6 Feb. 2011). NRCS, Washington, DC.

Odening, W.R., B.R. Strain, and W.C. Oechel. 1974. The effect of decreasing water potential on net CO_2 exchange of intact desert shrubs. Ecology 55:1086–1095. doi:10.2307/1940358

Philip, J.R., and D.A. de Vries. 1957. Moisture movement in porous materials under temperature gradient. Trans. Am. Geophys. Union 38:222–232.

Phillips, F.M. 1994. Environmental tracers for water movement in desert soils of the American Southwest. Soil Sci. Soc. Am. J. 58:15–24. doi:10.2136/sssaj1994.03615995005800010003x

Saito, H., J. Šimůnek, and B.P. Mohanty. 2006. Numerical analysis of coupled water, vapor, and heat transport in the vadose zone. Vadose Zone J. 5:784–800. doi:10.2136/vzj2006.0007

Sakai, M., N. Toride, and J. Šimůnek. 2009. Water and vapor movement with condensation and evaporation in a sandy column. Soil Sci. Soc. Am. J. 73:707–717. doi:10.2136/sssaj2008.0094

Scanlon, B.R., K. Keese, R.C. Reedy, J. Šimůnek, and B.H. Andraski. 2003. Variations in flow and transport in thick desert vadose zones in response to paleoclimactic forcing (0–90 kyr): Field measurements, modeling, and uncertainties. Water Resour. Res. 39(7):1179. doi:10.1029/2002WR001604.

Scanlon, B.R., D.G. Levitt, R.C. Reedy, K.E. Keese, and M.J. Sully. 2005a. Ecological controls on water-cycle response to climate variability in deserts. Proc. Natl. Acad. Sci. 102:6033–6038.

Scanlon, B.R., and P.C.D. Milly. 1994. Water and heat fluxes in desert soils: 2. Numerical simulations. Water Resour. Res. 30:721–733.

Scanlon, B.R., R.C. Reedy, K.E. Keese, and S.F. Dwyer. 2005b. Evaluation of evapotranspirative covers for waste containment in arid and semiarid regions in the southwest USA. Vadose Zone J. 4:55–71.

Šimůnek, J., M. Šejna, H. Saito, M. Sakai, and M.Th. van Genuchten. 2008. The HYDRUS-1D software package for simulating the movement of water, heat, and multiple solutes in variably saturated media, Version 4.0. HYDRUS Softw. Ser. 3. Dep. of Environ. Sci., Univ. of California, Riverside.

Smith, R.L. 1974. Ecology and field biology. 2nd ed. Harper and Row, New York.

Smith, S.D., R.K. Monson, and J.E. Anderson. 1997. Physiological ecology of North American desert plants. Springer-Verlag, Berlin.

van Genuchten, M.Th. 1980. A closed-form equation for predicting the hydraulic conductivity of unsaturated soils. Soil Sci. Soc. Am. J. 44:892–898. doi:10.2136/sssaj1980.03615995004400050002x

Walvoord, M.A., M.A. Plummer, F.M. Phillips, and A.V. Wolfsberg. 2002. Deep arid system hydrodynamics: 1. Equilibrium states and response times in thick desert vadose zones. Water Resour. Res. 38(12):1308. doi:10.1029/2001WR000824

Walvoord, M.A., D.A. Stonestrom, B.J. Andraski, and R.G. Striegl. 2004. Constraining the inferred paleohydrologic evolution of a deep unsaturated zone in the Amargosa Desert. Vadose Zone J. 3:502–512.

Yin, J., M.H. Young, and Z. Yu. 2008. Effects of paleoclimate and time-varying canopy structures on paleowater fluxes. J. Geophys. Res. 113:D06103. doi:10.1029/2007JD009010

Young, M.H., W. Albright, K.F. Pohlmann, G. Pohll, W.H. Zachritz, S. Zitzer, D.S. Shafer, I. Nester, and L. Oyelow. 2006. Incorporating parametric uncertainty in the design of alternative landfill covers in arid regions. Vadose Zone J. 5:742–750. doi:10.2136/vzj2005.0112